≪Research Paper≫ Applied Science and Convergence Technology Vol.23 No.5, September 2014, pp.265~272
http://dx.doi.org/10.5757/ASCT.2014.23.5.265

Numerical Investigation of RF Pulsing Effect on Ion Energy Distributions at RF-biased Electrodes

Deuk-Chul Kwon*, Mi-Young Song, and Jung-Sik Yoon

Plasma Technology Research Center, Nation Fusion Research Institute, Gunsan 573-540

(Received September 15, 2014, Revised September 29, 2014, Accepted September 30, 2014)

The ion energy distributions (IEDs) arriving at a substrate strongly affect the etching rates in plasma etching processes. In order to determine the IEDs accurately, it is important to obtain the characteristics of radio frequency (rf) sheath at pulsed rf substrates. However, very few studies have been conducted to investigate pulsing effect on IEDs at multiple rf driven electrodes. Therefore, in this work, we extended previous one-dimensional dynamics model for pulsed-bias electrodes. We obtained the IEDs using the developed rf sheath model and observed that numerically solved IEDs are in a good agreement with the experimental results.

Keywords : Sheath, Numerical modeling, ICP

I. Introduction

Pulsed radio frequency (rf) plasma sources are widely used for etching processes due to the marked improvement in etch characteristics to meet the stringent requirement of microelectronics fabrications [1-4]. It is well known that pulsing provides more flexibility for tuning an etch process by introducing new reactor control parameters such as the pulsing frequency, the duty cycle of the pulses, and the phase between the source pulses and the bias pulses. Accordingly, many research groups have been researching the pulsed plasmas by using the experimental and computational investigations [5-9]. Subramonium et al. [10] shown that the azimuthal uniformity of plasma parameters generally improved relative to continuous wave (cw) operations when decreasing duty cycle or pulse repetition frequency due to the longer afterglow period in Ar and Cl_2 plasmas. Agarwal et al. [2] and Subramonium et al. [11] found the extractions of negative ions from pulsed capacitively and inductively coupled plasma sources, respectively. Effects of rf bias pulsing on SiO_2 feature etching in fluorocarbon plasmas were investigated by Schaepkens et al. [12]. The authors of Ref. [12] obtained that the etch rate of any blanket substrate depends only on the pulse duty cycle and the ratio for fluorocarbon deposition rate to fluorocarbon etch rate. Banna et al. [13,14] shown that one can control the etching uniformity and profile in advanced gate etching, and reduce the leakage current by varying the synchronous pulsed plasma parameters. Moreover, the authors of Ref. [13] shown that synchronous pulsing has the promise of significantly reducing the electron shading effects compared with source pulsing mode and cw mode. Song et al. [15] found varying the size of a blocking capacitor is an additional variable which provides flexibility in con-

* [E-mail] dckwon@nfri.re.kr

trolling the shape of the ion energy distributions (IEDs).

The IEDs arriving at the substrate strongly affect the etch rates in plasma etching processes. In order to accurately determine the IEDs, various experimental methods and numerical models have been developed. Voronin et al. [16] obtained the time-resolved IEDs in a pulsed plasma using a quadrupole mass energy analyzer. Brihoum et al. [17] measured the ion flux and time-averaged IEDs for pulsed inductively coupled rf plasmas by using a retarding field analyzer. Also, using the similar approach, Shin et al. [18] measured the IEDs on a grounded substrate for cw and pulsed plasmas. The authors of Ref. [18] investigated that the peaks of the IEDs were controlled by adjusting the applied direct current (dc) bias and the discharge pressure. Dai et al. [19] and Barnat and Lu [20] presented a self-consistent fluid model which included all time-dependent terms in the ion fluid equations for pulsed dc bias. Diomede et al. [21] developed a model allowing rapid calculation of the IEDs on an electrode immersed in plasma for given voltage waveform applied to the electrode through a blocking capacitor. The model combined an equivalent circuit representation of the system with an equation for a damped sheath potential to which ions respond. In particular, Hong and co-workers [22] presented a hybrid model which was used to simulate the characteristics of collisional sheath in a capacitively coupled plasma driven by a dual frequency source including a rf and a pulsed dc to the same electrode.

In spite of the fact that various experimental method and numerical models have been suggested to obtain the IEDs, very few studies have been conducted on investigation of rf pulsing effect on IEDs at multiple rf driven electrodes. Therefore, in this work, we extended previous one-dimensional dynamics model for multiple rf modulated electrodes. The extended model was based on the previously developed models and an equivalent circuit model to determine the plasma potential and the potential drop within the sheath region. We obtained the time-averaged IEDs using the developed rf sheath model and observed that numerically solved IEDs are in a good agreement with the experimental results.

This paper is organized as follows. In Sec. II, model equations and a equivalent circuit model based on the rf sheath model are described. Results from some specific applications are presented in Sec. III. Finally, our conclusions are given in Sec. IV.

II. Model Description

1. Sheath model

We considered a one-dimensional plasma sheath treating electrons and negative ions as thermal Boltzmann particles but positive ions as cold fluids. The sheath edge at $x = x_s$ is the plasma-sheath interface, i.e. $x > x_s$ is the presheath and the plasma regions and $x < x_s$ is the sheath region [23,24].

The one-dimensional spatiotemporal variations of ion density, electron density, ion velocity, and electric potential are described by the ion continuity equation, the Boltzmann relation, the momentum equation, and the Poisson's equation, respectively:

$$\frac{\partial n_i}{\partial t} + \frac{\partial (n_i u_i)}{\partial x} = 0, \tag{1}$$

$$\frac{\partial u_i}{\partial t} + u_i \frac{\partial u_i}{\partial x} = -\frac{e}{m_i}\frac{\partial V}{\partial x}, \tag{2}$$

$$n_e = n_s \exp\left(\frac{eV}{k_B T_e}\right), \tag{3}$$

$$\frac{\partial^2 V}{\partial x^2} = -\frac{e}{\varepsilon_0}(n_i - n_e), \tag{4}$$

where n_i, u_i, and m_i are the density, velocity, and mass of ion species, respectively, e is the elementary charge, V is the potential, n_e is the electron density,

$k_B T_e$ is the electron temperature, and $n_s = n_0 \exp(e V_1/k_B T_e)$ [19]. Here, $V_1 = -k_B T_e/2e$ denotes the potential drop in the presheath and n_0 is the bulk plasma density [25].

We need to choose the suitable boundary conditions at the plasma-sheath interface to solve Eqs. (1)-(4). In this model, we define the similar boundary conditions as suggested by Dai et al. [19]. We assume that at the plasma-sheath boundary, the ion density should be equal to the electron density, i.e.,

$$n_i(x_s,t) = n_e(x_s,t) = n_0 \exp(eV_1/k_B T_e). \quad (5)$$

For cw bulk plasma, n_0 and $k_B T_e$ are constant in time. On the other hand, for source pulse operation we could not assume that n_0 and T_e are constant in time. Therefore, to investigate the effect of simultaneous source $n_0(t)$ and $k_B T_e(t)$ bias pulsing, time dependent and are determined by solving a global transport equation set. The detailed model used in this work are described in Sec. II.B. The obtained plasma parameters are used for density and electron temperature boundary conditions. Then the ion density at the plasma-sheath boundary can be rewritten as

$$n_i(x_s,t) = n_e(x_s,t) = n_0(t)\exp(-0.5). \quad (6)$$

We also assume that ions enter the sheath with a velocity equal to the Bohm velocity, i.e.,

$$u_i(x_s,t) = \sqrt{k_B T_e(t)/m_i}. \quad (7)$$

Finally, we assume that the potential at the sheath edge is zero, i.e.,

$$V(x_s,t) = 0, \quad (8)$$

and the potential at the electrode is equal to and instantaneous voltage, i.e.,

$$V(0,t) = V_s(t), \quad (9)$$

where V_s is obtained by coupling Eqs. (1)-(4) to a current balance equation.

Assuming sinusoidal voltage sources as shown in Fig. 1, the current balance at the substrate can be written as

$$\sum_i J_i - J_e - \frac{C_s(t)}{A}\frac{dV_s(t)}{dt} - \frac{V_s(t)}{A}\frac{dC_s(t)}{dt} = -\sum_l \frac{C_l^b}{A}\frac{d}{dt}[P_l V_l \sin(\omega_l t) - V_s(t)], \quad (10)$$

where J_i and J_e are the conduction current densities of the ion and electron, respectively, $C_s(t)$ is the sheath capacitance, A is the surface area of the substrate, and V_s is the electrode potential [19,24]. Using a similar approach based on Diomede et al. [21], the analytical expression for the applied voltage is presented by $P_l V_l \sin(\omega_l t)$ where V_l and ω_l are the voltage amplitude and the angular frequency of lth rf bias, respectively, and

$$P_l = 2 - \frac{1}{\exp[(t - t_l^0)/\Delta t] + 1} - \frac{1}{\exp[(-t + t_l^1)/\Delta t] + 1} - \frac{1}{\exp[(t - t_l^2)/\Delta t] + 1}. \quad (11)$$

Here, $t_l^0 = k/f_l$, $t_l^1 = k/f_l + 0.01 d_l/f_l$, and $t_l^2 = k/f_l + 1/f_l$. f_l and d_l are the pulse frequency and the duty ratio of lth rf bias, respectively, and k=(pulse period-1).

Moreover, assuming sinusoidal current source at

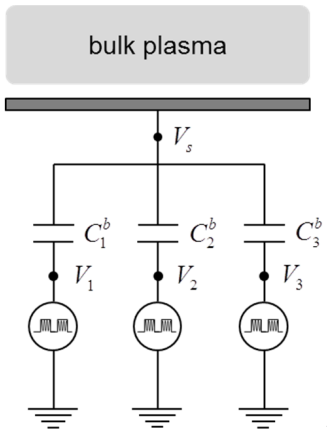

Figure 1. A schematic diagram of equivalent circuit for rf sheath model.

the electrode, the current balance can be rewritten as

$$\sum_i J_i - J_e - \frac{C_s(t)}{A}\frac{dV_s(t)}{dt} - \frac{V_s(t)}{A}\frac{dC_s(t)}{dt} = \sum_l P_l J_l \sin(\omega_l t), \quad (12)$$

where J_l is the amplitude of current density of lth rf bias. In this work, we adopted not only voltage driven but also current driven conditions to solve the current balance equation. The current balance is coupled to the sheath model through the electrode potential and the sheath thickness. By solving the current balance equation with the fourth order Runge-Kutta method, we obtain the potential drop across the sheath. Using the obtained potential $V_s(t)$, we then solve Eqs. (1)-(4) by using a finite difference method with an iterative process.

We assume that the time averaged power flowing from the rf bias power into the discharge is totally absorbed within the sheath region because the impedance of the bulk plasma is quite small comparing with the sheath impedance for the high-density and low-pressure plasmas. Therefore, the rf bias power to the substrate can be calculated from the time dependent voltage and current wave forms as

$$\overline{P}_l^{bias} = \frac{1}{\tau_l^{on}}\int_0^{\tau_l^{on}} V_s(t) I_s(t) dt, \quad (13)$$

where τ_l^{on} is the on-time of lth rf bias and $I_s(t)$ is the current on the electrode. Until each $\overline{P}_l^{bias}$ becomes equal to the applied lth rf bias power of P_l^{bias} within the margin of error, the amplitude of the applied rf current or voltage is determined by Eq. (13) with an iterative process. We found that the amplitude of applied rf current was unconditionally converged to obtain the applied power for current driven conditions. However, for voltage driven conditions, the initial amplitude of the applied rf voltage was highly sensitive to obtain the applied power.

2. Global transport model

Due to investigate the effect of simultaneous source and bias pulsing, we numerically solved the spatially averaged continuity equation and electron temperature equation based on Ar plasma chemistry [26]. The governing equations of the spatially averaged global model are as follows:

$$\frac{\partial n_i}{\partial t} = \sum_j R_{g,j} + \frac{Q_i}{\Omega} - \sum_j R_{l,j} - n_i\left(\frac{V_{pump}}{\Omega} + \nu_l^i\right), \quad (14)$$

$$\frac{\partial}{\partial t}\left(\frac{3}{2} n_e T_e\right) = \frac{P_{abs}}{\Omega} - \sum_j E_{e,j} - n_e \varepsilon_{e,l} \nu_l^e, \quad (15)$$

where $R_{g,j}$ and $R_{l,j}$ are the reaction rates of the various generation and loss processes of the species i, respectively. n_i is the density of species i particle, n_e is the electron density, Q_i is the gas flow rate of species i, Ω is the volume of the chamber, and V_{pump} is the pumping speed. The loss speed of the ions at the plasma-sheath boundary is assumed to be the Bohm velocity, thus the loss frequency of the ith ions species becomes $\nu_l^i = S\sqrt{T_e/m_i}/\Omega$. Here, S is the surface area of the chamber, T_e is the electron temperature, and M_i is the ion mass. Assuming the ambipolar diffusion, the loss frequency of the escaping electron into the wall is given $\nu_l^e = \sum_i \nu_l^i$. $E_{e,j}$ and $\varepsilon_{e,j}$ are the energy loss term from the electron per collision and the loss energy into the wall, respectively.

To simplify the analysis, we assumed that the absorbed power in Eq. (15) is modulated by an ideal rectangular waveform

$$P_{abs} = \begin{cases} P_{\max} & 0 \le t < \eta\tau \\ P_{\min} & \eta\tau \le t < \tau \end{cases}$$

where η and τ are the duty ratio and the period of source pulse, respectively [27].

III. Results

In Sec. II, we described the sheath model and the global transport model. By solving the nonlinearly coupled equations Eqs. (1)-(4) with fourth-order Runge-Kutta method, we obtained the potential and the ion energy at the electrode. The default plasma parameters used in these calculations are $Ar^{+}=10^{16}m^{-3}$ and $T_e = 3$ eV. We used these base values of the input parameters excluding the additional conditions given for the particular cases.

Fig. 2 shows the electrode potentials as function of normalized time for (A) 500 V at 2 MHz, (b) 500 V at 2 MHz and 100 V at 10 MHz, and (c) 500 V at 2 MHz, 100 V at 10 MHz, and 50 V at 60 MHz under 5 kHz and 50 % duty ratio of bias pulse operation. Here, the sinusoidal voltage source boundary conditions were applied for rf bias. After the bias powers turned off, the potentials decay toward constant values within two rf cycles.

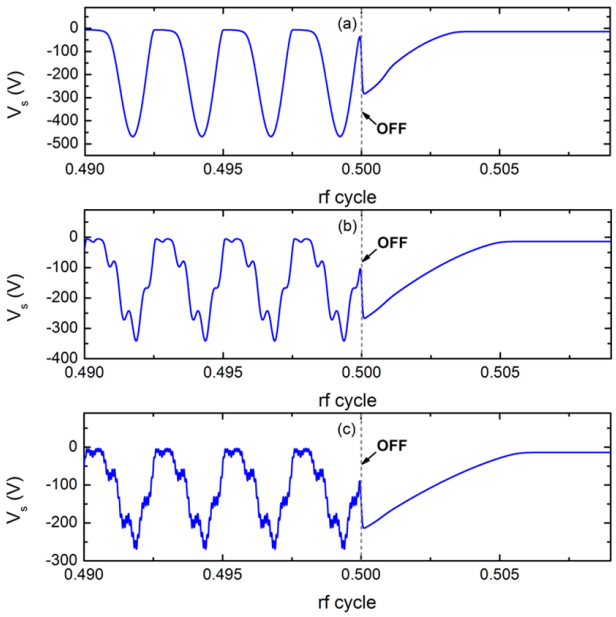

Figure 2. The electrode potentials as function of normalized time for (A) 500 V at 2 MHz, (b) 500 V at 2 MHz and 100 V at 10 MHz, and (c) 500 V at 2 MHz, 100 V at 10 MHz, and 50 V at 60 MHz under 5 kHz and 50% duty ratio of bias pulse operation. Other conditions: 5 nF blocking capacitance, $Ar^{+}=10^{16}m^{-3}$, and T_e=3 eV.

At the substrate, dependence of the time-averaged IEDs on duty ratio under 100 V at 10 MHz, 10 nF blocking capacitance, and 5 kHz bias pulse operation is shown in Fig. 3. We directly calculated the IEDs on the electrode using the formula

$$IEDs(E_i) \propto \sum_j \left[\frac{dm_i u_i^2/2}{dt_j} \right]^{-1}, \quad (16)$$

where j is the energy interval and E_i is the ion energy at the substrate. We can see that the height of the low-energy peak decreases as the duty ratio increases. Although the intensity of the energy is negligible, the amount of high energy ions increases as the duty ratio increases.

Due to investigate the effect of the blocking capacitor and rf frequency on the ion energy, as shown Fig. 4, we calculated temporal profiles of the ion energy at the substrate for (A) 500 V at 2 MHz, (b) 100 V at 10 MHz, and (c) 50 V at 60 MHz under 5 kHz bias pulse operation. We can see that the ion energy dramatically increases and decreases after the bias pow-

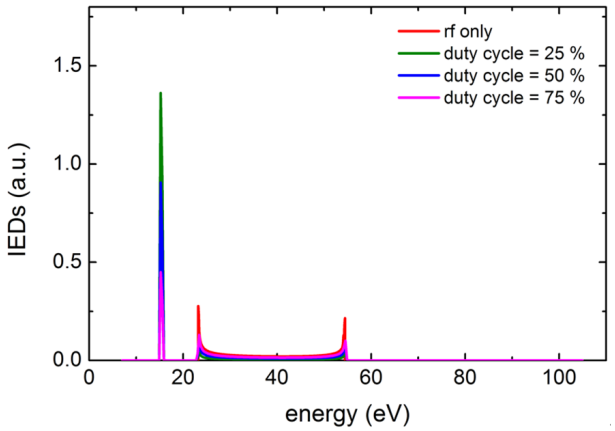

Figure 3. Dependence of the time-averaged IEDs at the electrode on duty ratio under 5 kHz bias pulse and cw source operation. Other conditions: 100 V at 10 MHz, 10 nF blocking capacitance, $Ar^{+}=10^{16}m^{-3}$, and T_e=3 eV.

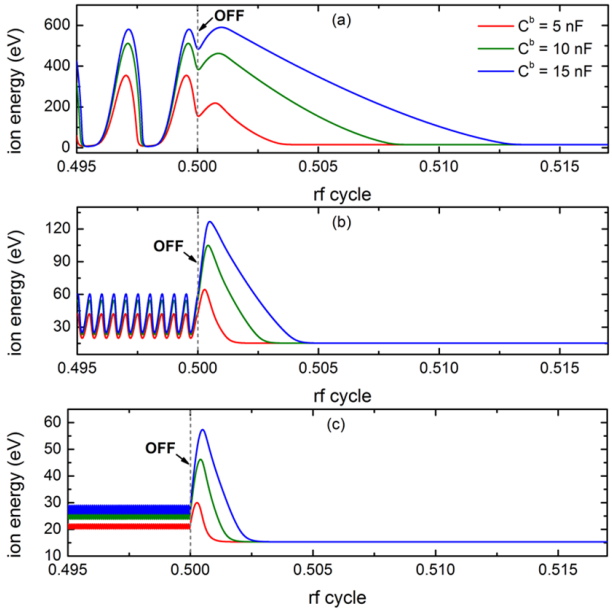

Figure 4. Temporal profiles of the Ar energy at the substrate for (a) 500 V at 2 MHz, (b) 100 V at 10 MHz, and (c) 50 V at 60 MHz under 5 kHz bias pulse operation. Plasma conditions are the same as that in Fig. 3.

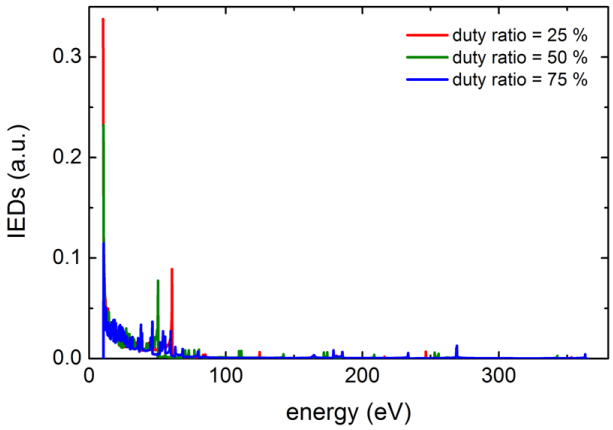

Figure 5. Dependence of the time-averaged IEDs at the electrode on duty ratio under 200 W at 2 MHz (5 kHz pulsing), 100 W at 10 MHz (cw), 50 W at 60 MHz (5 kHz pulsing), Ar^+=7.4×10^{16}m^{-3}, and T_e=2.7 eV.

ers turned off and the temporal profiles of the ion energy depend on the blocking capacitor. Because the ion density slowly responses to the applied modulated voltage in Eq. (10), after the bias powers turned off the ion conduction current increases and decreased to

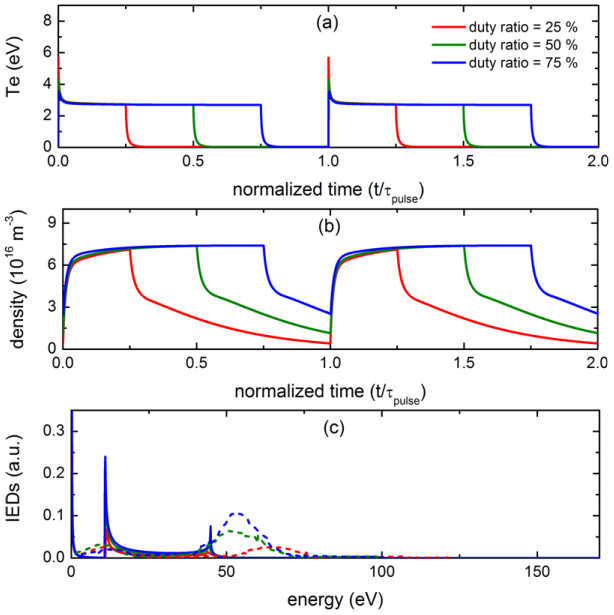

Figure 6. Temporal profiles of (a) the electron temperature and (b) the Ar^+ density and (c) time-averaged IEDs at the substrate. Chamber geometry and external conditions are the same as that in Ref. Brihoum. Solid and dashed lines are obtained value from simulation and experiment [17], respectively.

satisfy the current balance at the substrate. As a result, even though the intensity of the energy is negligible in the viewpoint of the time-averaged IEDs, higher energy ions arrive at the substrate than cw conditions as shown in Fig. 3.

Fig. 5 shows dependence of the time-averaged IEDs at the substrate on duty ratio under 200 W at 2 MHz (5 kHz pulsing), 100 W at 10 MHz (cw), 50 W at 60 MHz (5 kHz pulsing), and cw source operation. Here, Ar^+=7.4×10^{16}m^{-3} and T_e=2.7 eV were obtained by solving the global transport equation set under the same conditions in Ref. Brihoum. In this work, we found that the amplitude of applied rf current was unconditionally converged to obtain the applied power for current driven conditions. However, for voltage driven conditions, the initial amplitude of the applied rf voltage was sensitive to obtain the applied power. Therefore, with assuming the sinusoidal current source in Fig. 5, the amplitude of the applied rf cur-

rent were determined in a self-consistently manner.

To compare with the experimental result in Ref. [17], we numerically solved the spatially averaged continuity equation. Time dependent boundary conditions for the sheath module were obtained by solving the global transport equation. Figs. 6(a) and 6(b) show the obtained time variations of the electron temperature and the Ar^+ density, respectively. Here, chamber geometry and external conditions are the same as that in Ref. Brihoum. The total pressure is 10 mTorr with gas flow rate of 50 sccm, the ICP source power is 750 W, and 50 W wafer-chuck bias power is applied and pulsed at 1 kHz in phase with the ICP pulses. Fig. 6(c) shows the time-averaged IEDs for synchronously pulsed plasmas. Although there is a difference in the peak positions, numerically solved IEDs are in a good agreement with the experimental results.

IV. Conclusions

We extended previous one-dimensional dynamics model for multiple rf modulated bias power. The extended model was based on the previously developed models and an equivalent circuit model to determine the plasma potential and the potential drop within the sheath region. We obtained the time-averaged IEDs using the developed rf sheath model and observed that numerically solved IEDs are in a good agreement with the experimental results.

Although we considered single species ion for simplicity, in this work, the developed model should apply for multicomponent plasmas. However, we ignored the collisions within the sheath region. Therefore we will take into account the collisional effects on the motion of ions in the sheath region and use our model calculate the etch rates; this is under active study and will be reported later.

Acknowledgements

This work was supported by the Industrial Strategic Technology Development Program (10041637, Development of Dry Etch System for 10 nm class SADP Process) funded by the Ministry of Knowledge Economy (MKE, Korea) and also was supported by 2013 R&D Convergence Program funded by Korea Research Council of Fundamental Science & Technology (R&D Convergence-13-5-NFRI).

References

[1] A. Agarwal, P. J. Stout, S. Banna, S. Rauf, K. Tokashiki, J. Y. Lee, and K. Collins, J. Appl. Phys. **106**, 103305 (2009).

[2] A. Agarwal, S. Rauf, and K. Collins, J. Appl. Phys. **112**, 033303 (2012).

[3] S. Banna, A. Agarwal, G. Cunge, M. Darnon, E. Pargon, and O. Joubert, J. Vac. Sci. Technol. A **30**, 040801 (2012).

[4] A. Agarwal, P. J. Stout, S. Banna, S. Rauf, and K. Collins, Appl. Phys. Lett. **100**, 044105 (2012).

[5] T. H. Ahn, K. Nakamura, and H. Sugai, Plasma Sources Sci. Technol. **5**, 139 (1996).

[6] B. Ramamurthi and D. J. Economou, J. Vac. Sci. Technol. A **20**, 467 (2001).

[7] S. A. Voronin, M. R. Alexander, and J. W. Bradley, Meas. Sci. Technol. **15**, 2375 (2004).

[8] A. Agarwal, S. Rauf, and K. Collins, Appl. Phys. Lett. **99**, 021501 (2011).

[9] P. Subramonium and M. J. Kushner, Appl. Phys. Lett. **79**, 2145 (2001).

[10] P. Subramonium and M. J. Kushner, J. Appl. Phys. **96**, 82 (2004).

[11] P. Subramonium and M. J. Kushner, J. Vac. Sci. Technol. A **22**, 534 (2004).

[12] M. Schaepkens, G. S. Oehrlein, and J. M. Cook, J. Vac. Sci. Technol. B **18**, 856 (2000).

[13] S. Banna, A. Agarwal, K. Tokashiki, H. Cho, S. Rauf, V. Todorow, K. Ramaswamy, K. Collins, P. Stout, J. Y. Lee, J. Yoon, K. Shin, S. J. Choi, H. S. Cho, H. J. Kim, C. Lee, and D. Lymberopoulos, IEEE Trans. Plasma Sci. **37**, 1730 (2009).

[14] K. Tokashiki, H. Cho, S. Banna, J. Y. Lee, K. Shin, V. Todorow, W. S. Kim, K. H. Bai, S. H. Joo, J. D. Choe, K. Ramaswamy, A. Agarwal, S. Rauf, K. Collins, S. J. Choi, H. Cho, H. J. Kim, C. Lee, D. Dymberopoulos, J. Yoon, W. Han, and J. T. Moon, Jpn. J. Appl. Phys. **48**, 08DH01 (2009).

[15] S. H. Song and M. J. Kushner, J. Vac. Sci. Technol. A **32**, 021306 (2014).

[16] S. A. Voronin, M. R. Alexander, and J. W. Bradley, Meas. Sci. Technol. **16**, 2446 (2005).

[17] M. Brihoum, G. Cunge, M. Darnon, D. Gahan, O. Joubert, and N. St. J. Braithwaite, J. Vac. Sci. Technol. A **31**, 020604 (2013).

[18] H. Shin, W. Zhu, L. Xu, V. M. Donnelly, and D. J. Economou, Plasma Sources Sci. Technol. **20**, 055001 (2011).

[19] Z. L. Dai and Y. N. Wang, J. Appl. Phys. **92**, 6428 (2002).

[20] E. V. Barnat and T. M. Lu, Phys. Rev. E **66**, 056401 (2002).

[21] P. Diomede, D. J. Economou, and V. M. Donnelly, J. Appl. Phys. **111**, 123306 (2012).

[22] H. Zhang, Z. L. Dai, and Y. N. Wang, Plasma Sci. Technol. **13**, 513 (2011).

[23] P. A. Miller and M. E. Riley, J. Appl. Phys. **82**, 3689 (1997).

[24] T. Panagopoulos and D. J. Economou, J. Appl. Phys. **85**, 3435 (1999).

[25] A. Metze, D. W. Ernie, and H. J. Oskam, J. Appl. Phys. **60**, 3081 (1986).

[26] D. C. Kwon, W. S. Chang, M. Park, D. H. You, M. Y. Song, S. J. You, Y. H. Im, and J.-S. Yoon, J. Appl. Phys. **109**, 073311 (2011).

[27] M. A. Lieberman and A. J. Lichtenberg, *Principle of Plasma Discharges and Materials Processing*, 2nd ed. (Wiley, New York, 2004).